

Nearby Spiral Galaxy Globular Cluster Systems II: Globular Cluster Abundances in NGC 300^{1,2,3}

Julie B. Nantais and John P. Huchra

Harvard-Smithsonian Center for Astrophysics

60 Garden Street, Cambridge, MA 02138

Pauline Barmby

University of Western Ontario

London, ON N6S 3K7, Canada

and

Knut A. G. Olsen

Cerro-Tololo Inter-American Observatory, National Optical Astronomy Observatory

Casilla 603, La Serena, Chile

ABSTRACT

We present new metallicity estimates for globular cluster candidates in the Sd spiral NGC 300, one of the nearest spiral galaxies outside the Local Group. We have obtained optical spectroscopy for 44 Sculptor Group globular cluster candidates with the Boller and Chivens (B&C) spectrograph on the Baade Telescope at Las Campanas Observatory. Nine of these objects appear to be genuine old globular clusters, and six objects have spectral features consistent with either stars or globular clusters. (Because NGC 300 is a very nearby galaxy, one

¹Data for this project were obtained at the Baade 6.5 m telescope, Las Campanas Observatory, Chile.

²This study uses observations from the Hubble Space Telescope obtained at the Space Telescope Science Institute, operated by the Association of Universities for Research in Astronomy, Inc., under NASA contract NAS 5-26555. These observations are associated with Programs G0-9162, G0-9492, and G0-10915.

³This publication makes use of data products from the Two Micron All Sky Survey, which is a joint project of the University of Massachusetts and the Infrared Processing and Analysis Center/California Institute of Technology, funded by the National Aeronautics and Space Administration and the National Science Foundation.

cannot distinguish stars from globular clusters based on radial velocity alone.) The remaining candidates were stars, galaxies, and an HII region. One globular cluster, four galaxies, two stars, and the HII region were also identified in archival Hubble Space Telescope images. For the likely globular clusters, we measure spectral indices and estimate metallicities using an empirical calibration based on Milky Way globular clusters. The globular cluster system of NGC 300 appears similar to that of the Milky Way, but with a possible deficit in CN with respect to the Milky Way. Excluding possible stars and including clusters from the literature, the globular cluster system has a velocity dispersion of 67 km s^{-1} , and disk-like rotation is neither necessary nor ruled out. The mean metallicity for our full cluster sample plus one literature object is $[\text{Fe}/\text{H}] = -0.90$, lying above the relationship between mean globular cluster metallicity and overall galaxy luminosity. Excluding six candidates labeled as possible stars, we obtain a mean $[\text{Fe}/\text{H}] = -1.06$. Contamination from foreground stars in our cluster sample and color cuts eliminating blue objects may be responsible for the high metallicities. Visual confirmation of genuine globular clusters using high-resolution space-based imagery could greatly reduce the potential problem of interlopers in small samples of GC systems in low-radial-velocity galaxies.

Subject headings: galaxies: star clusters—galaxies: individual (NGC 300)—galaxies: spiral

1. Introduction

Globular clusters (GCs), relics of some of the earliest and/or most violent phases of star and galaxy formation, can be analyzed to understand how various types of galaxies formed, as described in the review by Brodie and Strader (2006). Two subpopulations of GCs, metal-rich (red) and metal-poor (blue), exist in most early-type galaxies. Both are thought to be old, but the red metal-rich GCs are thought to be slightly younger (Larsen et al. 2001; Kundu and Whitmore 1998; Lee, Kim, and Geisler 1998). Large spiral galaxies, including the Milky Way (Zinn 1985) and Andromeda (Barmby et al. 2000), also have metal-rich and metal-poor globular cluster subpopulations. In smaller, later-type galaxies, however, often only a metal-poor population is seen (Chandar et al. 2004). The most famous basic models for bimodal globular cluster system (GCS) formation in early type galaxies include dwarf galaxy accretion (Côté, Marzke, and West 1998), in situ formation (Forbes, Brodie, and Grillmair 1997), and gas-rich mergers (Ashman and Zepf 1992). In the last scenario, the original spiral galaxies - likely late-type spirals - would provide the entire metal-poor globular cluster population, and the metal-rich globular cluster population would form in the merger. Some evidence for globular clusters resulting from every one of

these processes exists, but the properties of both blue and red globular cluster populations have been found to scale with the mass of the host galaxy (Strader, Brodie, and Forbes 2004), indicating that the accretion model alone cannot account for the majority of blue globular clusters in bright galaxies. By comparing the GCS properties of potential elliptical-progenitor spiral galaxies with various elliptical galaxies, we can constrain the amount of globular cluster formation during a spiral-spiral merger and the era in which these mergers must have occurred.

Astronomers can also study old globular cluster populations that result from an initial burst of cluster formation to attack the problem of the age-metallicity degeneracy in the photometry and spectroscopy of stellar populations. Generally, one cannot distinguish whether youth or low chemical composition of a stellar population is responsible for the blue colors and certain spectral features associated with high average temperatures. However, once stellar populations reach an age of several Gyr, the effects of age on the color of the stellar population become small, making metallicity the primary source of color differences. Simple stellar population models (e.g. Worthey et al. 1994, Bruzual and Charlot 2003) predict very little change in color with age at advanced ages. We can therefore better determine metallicity differences in older stellar populations (such as globular clusters) than younger ones, allowing us to understand enrichment history as a function of Hubble type, galaxy luminosity, and formation environment.

The nearby Sculptor Group (or filament) is home to several late-type galaxies (Hubble types Sc–Im), including NGC 253 (the largest), NGC 300, NGC 55, and NGC 45. At a distance of 1.9 Mpc (Gieren et al. 2004), NGC 300 is one of the nearest spiral galaxies outside of the Local Group. As a nearby example of a late-type, midsize spiral galaxy, it is especially useful for understanding the sparse globular cluster systems of late-type galaxies. Kim et al. (2002) studied the star clusters in NGC 300 photometrically and identified 17 objects as globular cluster candidates based on their extent and color. Olsen et al. (2004) performed photometry on fields in six Sculptor Group galaxies and identified globular cluster candidates via shape and color. Of the shape-and-color-selected candidates that Olsen et al. analyzed spectroscopically, six had high enough signal-to-noise spectra for metallicity determination via Lick/IDS indices. Seven of the globular clusters Olsen et al. spectroscopically confirmed were in NGC 300, and two had spectroscopically determined metallicities.

In this paper we present new metallicities derived from spectroscopy of globular clusters in Sculptor Group galaxies, primarily NGC 300, using Kim et al. (2002) and Olsen et al. (2004) as reference catalogs. We compare the metallicities of NGC 300 globular clusters to those of Andromeda and Milky Way clusters, and also determine NGC 300’s place on the galaxy luminosity-GC system metallicity relation of Brodie and Huchra (1991).

2. Data reduction and cluster selection

We obtained spectra of 44 Sculptor Group cluster candidates taken with the Boller & Chivers (B&C) spectrograph on the Baade telescope from 2002 November 6 to 2002 November 9. We obtained spectra of all 17 globular cluster candidates from Kim et al. (2002), plus 27 Olsen et al. (2004) GC candidates, 25 of which are in NGC 300 and two of which are in NGC 253. The Olsen et al. candidates we observed were the brightest objects in the catalog with no previous spectroscopy (except for NGC 300-ax), and were observed roughly in order of increasing magnitude. Figure 1 shows the locations of the NGC 300 objects with respect to a schematic of the NGC 300 disk. Of the Olsen et al. clusters, 19 of the 27 are among the 38 Sculptor Group globular cluster candidates for which we also obtained *JHK* photometry with the PANIC camera on the Baade 6.5 m telescope (Nantais et al. 2006, Paper I).

The advantages of using the long-slit B&C spectrograph rather than a fiber spectrograph include good coverage in blue optical wavelengths, better sky subtraction (due to the sky background being determined at the same time and place as the object exposure), and the ability to adjust the slit width to the seeing to alleviate flux loss due to poor seeing. Also, the sky at Las Campanas has significantly weaker telluric emission lines than less isolated telescope locations. Our spectra were taken with the 600 l/mm grating blazed at 5000 Å. The wavelength range is about 3700-6860 Å. Their dispersion is 1.6 Å/pixel, and the resolution of the spectra is about 5 Å.

Bias subtraction (with an averaged bias image), dark count correction, and flatfielding were done with IRAF’s *ccdproc* task, and spectra were extracted using IRAF’s *apall* task. Other tasks in the *specred* and *onedspec* packages were used to combine spectra, calibrate wavelengths, flux-calibrate the spectra using standard star observations taken each night, and eliminate pollutants such as cosmic rays and improperly-subtracted telluric lines.

Velocities were determined with the *xcsao* task in the *rvsao* package (Kurtz and Mink 1998) in IRAF using a list of standard SAO templates useful for the expected features of globular clusters, background galaxies, and foreground stars. Included are four templates derived from M31 globular clusters (*m31_a_temp*, *m31_f_temp*, *m31_k_temp*, and *fglotemp*), three galaxy absorption templates (*fm32temp*, *habtemp90*, and *fn4486btemp*), two composite stellar absorption templates (*fabtemp97* and *fallstars*), a synthetic HII region/galaxy emission template (*hemtemp0.0*), and a synthetic Ca H&K absorption template (*hkabstemp*). For each object, we list a heliocentric velocity determined from the template with the highest R value.

We visually inspected the reduced, calibrated spectra to determine whether they were

globular clusters, probable globular clusters, stars, galaxies, HII regions, or unknown. Objects labeled as stars usually had the very strong magnesium and sodium features that one would expect from foreground K-dwarf stars. Objects labeled as clusters usually had spectra similar to G and K giants, but with less pronounced magnesium and sodium. Objects that had very low radial velocities (less than 0 km s^{-1} especially) and/or Mg and Na features that were fairly bright but not obviously stars were tagged as “gc or star.” Since the heliocentric radial velocity of NGC 300 is fairly low — $+142 \pm 4 \text{ km s}^{-1}$ (de Vaucouleurs et al. 1991) — it is impossible to eliminate all stars and keep all globular clusters in the sample if a strict velocity cut is used to exclude candidates. Hence, we cannot automatically label objects with clusterlike spectra but very low radial velocities as definite stars. The velocity dispersion in NGC 300’s halo is estimated by Carignan and Freeman (1985) to be 60 km s^{-1} . If the Milky Way halo were non-rotating, the average expected radial velocity of a Galactic star in the direction of NGC 300 would be about $+40 \text{ km s}^{-1}$, and the velocity dispersion of the Milky Way halo is about 130 km s^{-1} (as viewed from the center of the Milky Way). So while there’s a 95% chance that an NGC 300 halo object will have a radial velocity greater than 20 km s^{-1} , Milky Way halo stars can very easily have velocities similar to those of genuine NGC 300 globular clusters. This means that most objects with negative radial velocities will be Milky Way stars, but those with positive radial velocities could easily be either foreground stars or NGC 300 clusters, and only spectral features or high-resolution imaging can distinguish them.

The best-fit velocity template also hints at whether an object is likely to be a star or a cluster. Most GCs were best fit by F-type and K-type templates, while many foreground dwarfs were best fit by generic stellar templates such as “fallstars” and “fabtemp97.”

Background galaxies had highly redshifted Calcium H&K features and/or redshifted emission lines, and thus were easy to recognize. Figure 2 shows sample spectra of an old globular cluster, a foreground star, and a background galaxy, in which the stronger Mg and Na lines of the star compared to the globular cluster and the redshifted H&K lines of the galaxy are clearly visible.

3. Discovering Clusters

The names, heliocentric cross-correlation velocities, and object type (background galaxy, foreground star, cluster candidate) are shown in Table 1. The objects with number designations 1-17 are from Kim et al. 2002; the rest are from Olsen et al. 2004. Of the 17 Kim et al. candidates, only five — objects 2, 3, 4, 5, and 12 — appear to be old globular clusters. Note that object 3 is also NGC 300a in Olsen et al.’s catalog, and has been proven a globular

cluster and spectroscopically evaluated by Olsen and collaborators. Most of the remaining Kim et al. objects were background galaxies, except for one HII region (Object 6) and three probable NGC 300 stars (NGC 300-09, M-type; NGC 300-10, F-type; and NGC 300-15, A-type).

Since globular clusters in NGC 300 can easily be resolved with HST, we searched the HST ACS and WFPC2 archives for images of our NGC 300 objects. The images were from programs G0-8584, G0-9162, G0-9492, and G0-10915. We found eight Kim et al. objects in the archival HST images: Objects 1, 5, 6, 7, 8, 9, 10, and 11. These eight objects are shown in Figure 3. Generally, their appearances match what we expect based on their spectra. Objects 1, 7, and 11 are spiral galaxies; Object 8 is an early-type galaxy; Object 6 is an HII complex; Object 5 appears to be a genuine globular cluster; and Objects 9 and 10, initially considered as possible open clusters, appear pointlike but non-saturated and without diffraction spikes. Their Kim et al. (2002) V magnitudes are 19.73 for NGC 300-09 (which has an M-type spectrum) and 19.12 for NGC 300-10 (which has an F-type spectrum), consistent with supergiant stars in NGC 300.

Kim et al. selected their globular cluster candidates by using a color cut ($0.3 < B - V < 2.0$) and morphological considerations, including visual inspection of the shapes and brightness profiles. They assigned three “classes” to the quality of GC candidates, class 1 being most likely to be GCs and class 3 being least likely. Interestingly, only one of the Class 1 objects — Object 12 — turned out to be a globular cluster; the other three were background galaxies. This may be because, in images where globular clusters are barely resolved, the most highly resolved objects are very likely to be background galaxies.

Of the Olsen et al. candidates, 10 objects appeared to be stars, including NGC 300ax, which Olsen et al. had identified and analyzed as a globular cluster. Its spectrum has wide spectral lines consistent with a dwarf of late K to early M type: a wide but shallow Mg feature and a wide and deep Na feature. Both NGC 253 objects and two of the NGC 300 objects had all the features fully consistent with globular clusters, including high radial velocities and modest Mg and Na. Six more NGC 300 objects were labeled as “gc or star” due to either low radial velocity (3 had barycentric velocities below 0 km s^{-1}) or somewhat strong Mg and/or Na but not as strong as those of the obvious stars. All remaining objects were background galaxies.

4. Velocity Dispersion, Rotation, and Estimated Mass

Our GC velocities — 7 highly probable clusters and 6 possible clusters — can be combined with seven globular cluster velocities from Olsen et al. (2004) and unpublished data contributed by one of our collaborators (K. Olsen) to obtain a GC velocity dispersion and simple mass estimate for NGC 300. The velocities used in our analysis are listed in Table 2. Figure 4 shows the velocity histograms including and excluding the 6 candidates deemed possible stars.

If we include all highly probable and possible cluster candidates — 20 objects in all — we

have a mean velocity of 77 km s^{-1} and a velocity dispersion, corrected for the mean uncertainty of the velocities, of 89 km s^{-1} . If we exclude the six possible stars, we have 14 objects with a mean velocity of 113 km s^{-1} and an uncertainty-corrected velocity dispersion of 67 km s^{-1} . This latter dispersion resembles the Carignan and Freeman (1985) theoretical velocity dispersion estimate of 60 km s^{-1} .

We can also investigate whether there is evidence for rotation among our globular clusters. Figure 5 shows the velocity of cluster candidates as a function of position angle, along with a fit to the rotation of all candidates not labeled as possible stars and a representation of the Puche, Carignan, and Bosma (1990) HI rotation curve (with the velocity of 90 km s^{-1} reduced by a factor of $\sin(i)$ with $i = 42.3^\circ$). We fit a function of the form

$$V(\theta) = V_c + V_{pr} * \sin(\theta - \theta_0) \quad (1)$$

to the velocities and position angles of the 14 “good” clusters. V_c is the central velocity, V_{pr} is the projected rotational velocity (the actual rotational velocity times $\sin(i)$), θ is the position angle of the cluster in degrees measured east from north, and θ_0 is the position angle of the rotation axis. Using a nonlinear least-squares fit with weights equal to $1/\sigma_v^2$, we found $V_c = (122 \pm 22) \text{ km s}^{-1}$, $V_{pr} = (60 \pm 28) \text{ km s}^{-1}$, and $\theta_0 = (-6^\circ \pm 44^\circ)$, similar to the HI rotation curve. However, the uncertainty-corrected dispersion of the 14 GC velocities minus their predicted rotational velocities is still 66 km s^{-1} , essentially unchanged from our previous result. It is thus unclear from our data whether the NGC 300 GC system is rotating.

We use the Projected Mass Estimator (Heisler, Tremaine, and Bahcall 1985) to estimate the total mass of NGC 300, both using the means of the total and “good” samples and the mean velocity of NGC 300 itself. The equation for the projected mass estimator is as follows:

$$M_{PM} = \frac{f_{pm}}{G(N - \alpha)} \sum_i V_{zi}^2 R_{\perp i}. \quad (2)$$

Here we use $f_{pm} = 32/\pi$ (for isotropic orbits, recommended by Heisler, Tremaine, and Bahcall (1985) and $\alpha = 1.5$. Using the published mean velocity of NGC 300 itself gives $M_{PM} = (1.8 \pm 0.2) \times 10^{11} M_\odot$ for the total sample, and $M_{PM} = (8.1 \pm 0.7) \times 10^{10} M_\odot$ for the best-candidate subsample. Both samples reach a maximum distance of 13.7 kpc. Uncertainties were estimated using the jackknife method. Puche, Carignan, and Bosma (1990), using HI rotation curve data, calculate a mass of $2.4 \times 10^{10} M_\odot$ out to 10.6 kpc; Rhee and Chun (1992) give mass-model-based estimates for the mass of NGC 300 ranging from $2.8 - 4.2 \times 10^{10} M_\odot$. The mass-to-light ratio of galaxy groups can set an upper limit for the mass associated with a given galaxy; using the 2MASS K-band magnitude and the mass-to-light ratio of $72 M_\odot/L_\odot$ for galaxy groups calculated by Crook et al. (2007), this upper limit for NGC 300 would be about $1.7 \times 10^{11} M_\odot$. Overall, our masses run large but are not outside the realm of possibility.

5. Analysis of Chemical Abundances

We measured 25 spectral indices, including the 12 indices calibrated in Brodie and Huchra (1990) using the Brodie and Huchra (1990) bandpass definitions. Eight of these indices are mostly similar to the Lick/IDS bandpass definitions, differing slightly from those of Worthey et al. (1994) and Trager et al. (1998). The rest of the indices, those not in Brodie and Huchra (1990), were measured using the bandpass definitions of Trager et al. (1998). All bandpasses were shifted to the uncorrected, geocentric radial velocities of our objects. Our indices are not true Lick indices because our spectra have not been degraded to match the resolution of the Lick star spectra, and we did not observe any Lick standard stars to calibrate the fluxes and indices precisely. However, we did observe a template galaxy (NGC 1052) that was also observed by Brodie and Huchra (1990), and found the overlapping indices to be similar to theirs. All indices are given in magnitudes, as in Brodie and Huchra, for easy comparison with their M31 spectral indices and index-metallicity calibration methods. Converting to equivalent width requires multiplication by the bandwidth of the central index band shifted to the object’s velocity.

We determined metallicities using a method based on the Brodie and Huchra (1990) prescription, but with new index-vs.-metallicity calibrations determined from the 41 Milky Way spectra from Schiavon et al. (2005), degraded to match the 5 Å resolution of our spectra. We determined linear regressions for metallicity (from Harris (1996) for each Milky Way GC) as a function of index strength for all our indices, as well as the “range” R_I defined as in Brodie and Huchra (1990), and the σ_m representing the scatter about the regression line. We used the R_I and σ_m values to construct weights similar to those in Brodie and Huchra (1990):

$$W_I = \frac{R_I}{(\sigma_m^2 + \sigma_p^2 + \sigma_s^2)^{1/2}} \quad (3)$$

with σ_p being the photometric uncertainty in the entire index, the quadrature sum of the uncertainties in each band. To calculate σ_s , the measure of our ability to measure the same index repeatedly for the same object over the course of different nights and conditions, we used spectral index measurements for the standard star LTT 9239, which we observed each night. We modified the formula for the uncertainty in a band (continuum or feature value for an index) from Brodie and Huchra (1990) to the following:

$$snr = 1/\sigma_B = O/(O + S + R^2)^{1/2}, \quad (4)$$

where O is the number of object counts per pixel, S is the number of sky counts per pixel, and R is the read noise. The weighted average and uncertainty in the weighted average were determined as in Brodie and Huchra (1990).

Our choice of indices to use in the weighted average was determined by considering the correlation coefficient in each Milky Way linear fit, their signal-to-noise ratio in the NGC 300 objects, and the degree of scatter in NGC 300 index-index relations. The final set of indices - Mg2, Fe5270, Fe5335, Ca4227, G4300, δ , Ca4455, and CN2 - all had relatively high correlation coefficients in

the Milky Way index-metallicity relations and relatively high signal-to-noise in typical NGC 300 clusters.

Table 3 lists measurements and uncertainties of the 12 indices calibrated in Brodie and Huchra, and Table 4 gives the measurements and uncertainties of the remaining 13 indices. Table 5 lists the linear relationships between index and metallicity for the 8 indices we chose, and Table 6 lists derived metallicities for our clusters, along with five spectroscopically determined metallicities for Sculptor Group globular clusters from Olsen et al. (2004).

Figures 6-10 compare various spectral indices to those of Andromeda Galaxy GCs (Huchra, Brodie, and Kent 1991; Barmby et al. 2000) and the Schiavon et al. Milky Way GCs. Figure 6 shows that the CNR index lies below typical values for Andromeda and Milky Way clusters, while the CNB index, traditionally considered a more reliable indicator of CN abundance, looks about normal. Figure 7 shows a close-up of the CNB region for averages of 10 Milky Way and 10 NGC 300 objects matched for Fe52 strength. The CNB depths look fairly similar, although a tilt due to the high reddening of many of the MW GCs is visible. Fe52 abundances, as seen in Figure 8, look similar in all three galaxies. The G-band (Figure 9) seems about 0.02 mag high compared to the Milky Way and Andromeda, although overall more similar to the Milky Way. And finally, $H\beta$, the index that is sensitive to age and inversely correlated with metallicity, is shown in Figure 10. NGC 300 GCs show a mean and distribution more similar to the Milky Way than to Andromeda, suggesting old clusters similar to those of the Milky Way, which lacks young cluster population seen in Andromeda.

The deficit in CNR in our sample does not necessarily indicate a nitrogen deficiency in the globular clusters of NGC 300, especially given the apparently normal CNB. Andromeda globular clusters had once been thought to have nitrogen excesses compared to Milky Way GCs (Burstein et al. 1984; Brodie and Huchra 1991), but this was later challenged when the metal-rich Milky Way GCs were taken into account (Puzia et al. 2002). Instead, Puzia et al. found that metal-rich GCs in both Andromeda and the Milky Way were nitrogen-enhanced compared to the general old stellar populations of galaxies, which they propose may be due to low-mass globular cluster stars accreting carbon and/or nitrogen from the AGB winds of dying higher-mass stars in the cluster. A deficiency in CNR in our sample, therefore, may suggest a deficiency in true metal-rich globular clusters, suggesting that most of our apparently metal-rich objects may be Milky Way halo foreground stars, which should lack nitrogen compared to metal-rich globular clusters of similar metallicity. Four of the five objects that lie on the lower right on the CNR vs. Mg2 plot (Figure 4b), with Mg2 indices above +0.125 and lacking strong CNR, are among our six objects labeled as possible stars based on ambiguous spectral features. It may also be due to the fact that the CNR feature is quite weak, and our signal-to-noise ratios are not especially high.

Overall, these index patterns suggest a globular cluster system similar to that of the Milky Way.

Figure 11 shows the abundance distribution of the NGC 300 globular clusters as compared to the Milky Way, Andromeda, and M33, including NGC 300r from Olsen et al. (2004). With

all candidates included, the distribution appears bimodal, but if the six most starlike clusters are excluded, the distribution is effectively unimodal. With such a small sample, however, we cannot definitively determine bimodality.

An updated version of the Brodie and Huchra (1991) relation between mean globular cluster system (GCS) metallicity was created using relatively recent published galaxy distance and spectroscopic GC metallicity information from the literature on several galaxies and contemporary 2MASS K and de Vaucouleurs et al. (1991) B magnitudes found on NED. Table 7 summarizes the data, gathered from a wide variety of studies of globular cluster systems using different selection criteria. The relationship between the mean GCS metallicity and absolute B magnitude is shown in Figure 12, and relationship between mean GCS metallicity and absolute 2MASS K magnitude is shown in Figure 13. NGC 300, with its calculated mean GC metallicity of -0.90 ± 0.13 , lies above both the early-type and late-type galaxies on the plot. The high metallicity calculated for NGC 300 could be due to most of the “higher metallicity” cluster candidates being foreground stars, as suggested above in the discussion of CN deficiency. If the six clusters deemed to be possible foreground stars are eliminated, the mean metallicity of the remaining eight clusters (our seven clusters plus NGC 300r) is -1.06 ± 0.16 , which is still higher than expected for a galaxy the size of NGC 300. Besides possible foreground star contamination, color selection in the candidate samples may have created a bias in favor of metal-rich, intrinsically red clusters that drastically increases their relative numbers in our tiny sample. It is also worth noting that the spectroscopic metallicity estimates used in our metallicity-luminosity relations do not distinguish among the $[\alpha/Fe]$ values that may differ among different galaxy types.

6. Summary/Conclusions

The globular cluster system of NGC 300 appears to have chemical abundance properties similar to those of the Milky Way in age and relative abundances. Its place on the metallicity-luminosity relation is consistent with the positive correlation between galaxy luminosity and mean globular cluster metallicity, although the average metallicity of our NGC 300 cluster sample is higher than expected. Eliminating all ambiguous objects from our cluster sample gives a mean metallicity slightly more consistent with the Milky Way and Andromeda. The globular clusters, excluding those deemed possible stars, have a velocity dispersion of 67 km s^{-1} , similar to theoretical predictions, and may be rotating although the evidence is ambiguous. Small numbers, stellar contamination, and the possible tendency of color cuts to bias our object sample toward high metallicities all may contribute to the high mean metallicity of our NGC 300 cluster sample. The problem of mistaking foreground stars (and giant stars within the galaxy) for globular clusters could easily be remedied with more space-based imaging of NGC 300 to allow the visual recognition of star clusters, which can then be studied spectroscopically. Color cuts may also be less necessary when the clusters are well-resolved.

We would like to thank the LCO staff for helping us use the Magellan Telescopes and instruments. This work has been supported by the Smithsonian Institution and Harvard College Observatory. We also thank Ricardo Schiavon and collaborators for making their Milky Way spectra available to the public at <http://www.noao.edu/ggclib/>.

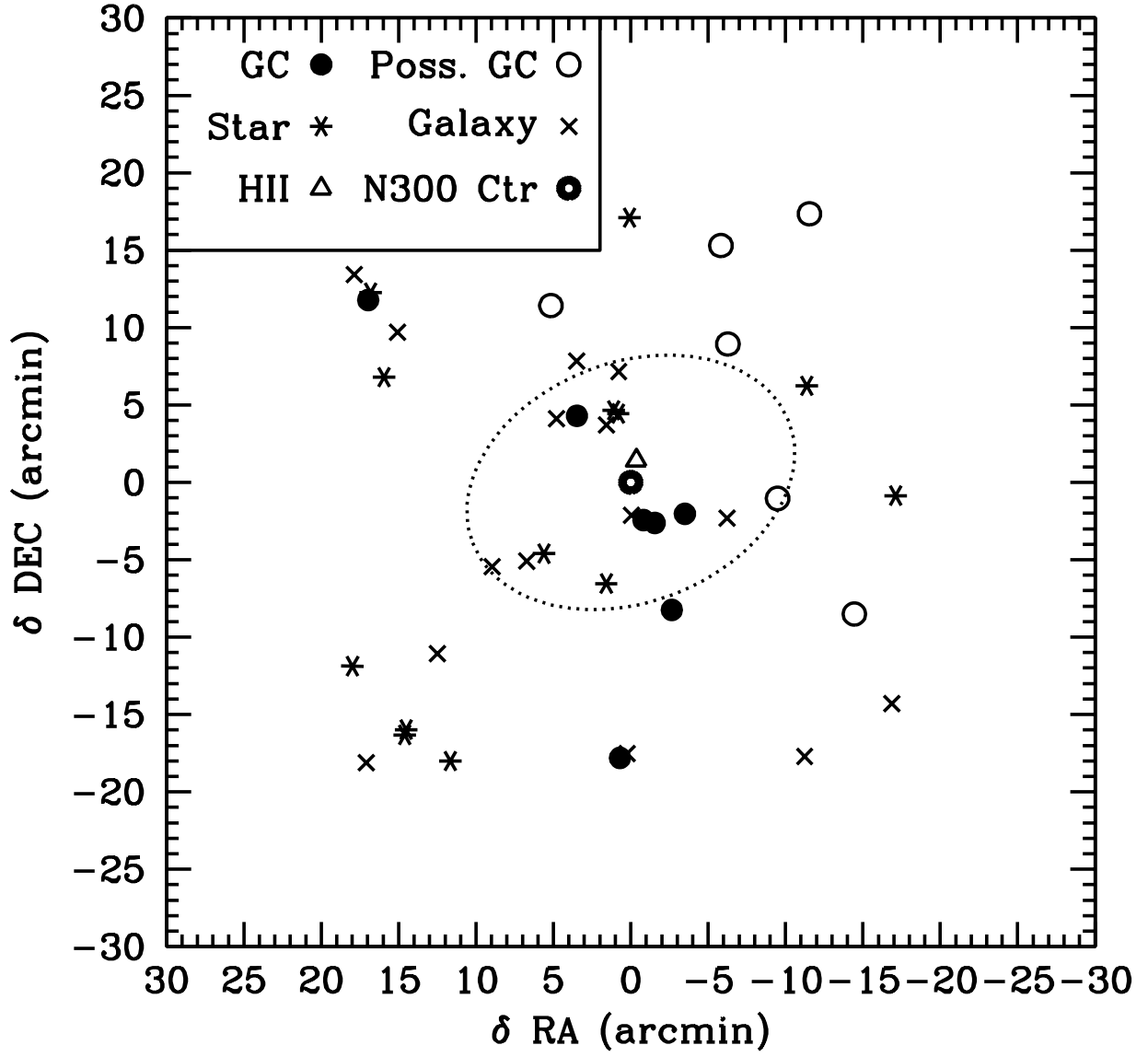
REFERENCES

- Ashman, K. M., and Zepf, S. E. 1992, *ApJ*, 384, 50.
- Barmby, P., Huchra, J. P., Brodie, J. P., Forbes, D. A., Schroder, L. L., and Grillmair, C. J., 2000, *AJ*, 119, 727.
- Beasley, M. A., Bridges, T., Peng, E., Harris, W. E., Harris, G. L. H., Forbes, D. A., Mackie, G. 2008, *MNRAS*, 386, 1443.
- Beasley, M. A., Forbes, D. A., Brodie, J. P., and Kissler-Patig, M. 2004, *MNRAS*, 347, 1150.
- Bersier, D. 2000, *ApJ*, 543, L23.
- Brodie, J. P., and Huchra, J. P. 1990, *ApJ*, 362, 503.
- Brodie, J. P., and Huchra, J. P. 1991, *ApJ*, 379, 157.
- Brodie, J. P., and Strader, J. 2006, *ARA&A*, 44, 193.
- Bruzual, G. and Charlot, S. 2003, *MNRAS*, 344, 1000.
- Burstein, D., Faber, S., Gaskell, M., and Krumm, N. 1984, *ApJ*, 287, 586.
- Cappellari, M. et al. 2006, *MNRAS*, 366, 1126.
- Carignan, C. and Freeman, K. C. 1985, *ApJ*, 294, 494.
- Chandar, R., Whitmore, B., and Lee, M. G. 2004, *ApJ*, 611, 220.
- Chomiuk, L., Strader, J., and Brodie, J. 2008, arXiv:0804.4472v1 [astro-ph]
- Cohen, J. G., Blakeslee, J. P., and Côté, P. 2003, *ApJ*, 592, 866.
- Côté, P., Marzke, R. O., and West, M. J. 1998, *ApJ*, 501, 554.
- Crook, A. C., Huchra, J. P., Martimbeau, N., Masters, K. L., Jarrett, T., and Macri, L. M. 2007, *ApJ*, 655, 790.
- de Vaucouleurs, G., de Vaucouleurs, A., Corwin Jr., H. G., Buta, R. J., Paturel, G., and Fouque, P. 1991, *Third Reference Catalog of Bright Galaxies, Version 3.9* (New York: Springer-Verlag)

- de Vaucouleurs, G. and Page, J. 1962, ApJ, 136, 107.
- Ferrarese, L. et al. 2000, ApJ, 529, 745.
- Forbes, D. A., Brodie, J. P., and Grillmair, C. J. 1997, AJ, 113, 1652
- Freedman, W. 1990, ApJ, 355, L35
- Freedman, W. L., Hughes, S. M., Madore, B. F., Mould, J. R., Lee, M. G., Stetson, P., Kennicutt, R. C., Turner, A., Ferrarese, L., Ford, H., Graham, J. A., Hill, R., Hoessel, J. G., Huchra, J., and Illingworth, G. D. 1994, ApJ, 427, 628.
- Galleti, S., Bellazzini, M., and Ferraro, F. R. 2004, *a*, 423, 925.
- Gieren, W., Pietrzyński, G., Walker, A., Bresolin, F., Minniti, D., Kudritzki, R., Udalski, A., Soszński, I., Fouqué, P., Storm, J., and Bono, G. 2004, AJ, 128, 1167.
- Harris, W. E. 1996, AJ, 112, 1487.
- Heisler, J., Tremaine, S., and Bachall, J. N. 1985, ApJ, 298, 8.
- Huchra, J. P., Brodie, J. P., and Kent, S. M. 1991, ApJ, 370, 495.
- Jarrett, T. H., Chester, T., Cutri, R., Schneider, S. E., and Huchra, J. P. 2003, AJ, 125, 525.
- Jensen, J. B., Tonry, J. L., Barris, B. J., Thompson, R. I., Liu, M. C., Rieke, M. J., Ajhar, E. A., and Blakeslee, J. P. 2003, ApJ, 583, 712.
- Kang, A., Kim, J., Shin, I., Chun, S., Kim, H., and Sohn, Y. 2007, JASS, 24, 203.
- Kim, S.C., Sung, H., and Lee, M.G. 2002, Journal of the Korean Astronomical Society, 35, 9.
- Kissler-Patig, M., Brodie, J. P., Schroder, L. L., Forbes, D. A., Grillmair, C. J., and Huchra, J. P. 1998, AJ, 115, 105.
- Kundu, A. and Whitmore, B. C. 1998, AJ, 116, 2841.
- Kurtz, M. J. and Mink, D. J. 1998, PASP, 110, 934.
- Larsen, S. S. and Brodie, J. P. 2002, AJ, 123, 1488.
- Larsen, S. S., Brodie, J. P., Beasley, M. A., and Forbes, D. A. 2002, AJ, 124, 828.
- Larsen, S. S., Brodie, J. P., Huchra, J. P., Forbes, D. A., and Grillmair, C. J. 2001, AJ, 121, 2974.
- Lauberts, A. and Valentijn, E. A. 1989, The Surface Photometry Catalogue of the ESO-Uppsala Galaxies (Garching Bei Munchen: ESO)
- Lee, M. G., Kim, E., and Geisler, D. 1998, AJ, 115, 947.

- Li, Y. and White, S. 2008, MNRAS, 384, 1459.
- McConnachie A.W., Irwin M.J., Lewis G.F., Ibata, R.A., Chapman, S.C. Ferguson A.M.N., Tanvir N., 2004, MNRAS, 351, L9
- Nantais, J. B., Huchra, J. P., Barmby, P., Olsen, K. A. G., and Jerret, T. H. 2006, AJ, 131, 1416.
- Norris, M. A., Sharples, R. M., Bridges, T., Gebhart, K., Forbes, D. A., Proctor, R., Raul Faifer, F., Carlos Forte, J., Beasley, M. A., Zepf, S. E., and Hanes, D. A. 2008, MNRAS, 385, 40.
- Olsen, K. A. G., Miller, B. W., Suntzeff, N. B., Schommer, R. A., and Bright, J. 2004, AJ, 127, 2674.
- Perelmuter, J., Brodie, J. P., and Huchra, J. P. 1995, AJ, 110, 620.
- Proctor, R. N., Forbes, D. A., Brodie, J. P., and Strader, J. 2008, MNRAS, 385, 1709.
- Puche, D., Carignan, C., and Bosma, A. 1990, AJ, 100, 1468.
- Puzia, T. H., Saglia, R. P., Kissler-Patig, M., Maraston, C., Greggio, L., Renzini, A., and Ortolani, S. 2002, *Å*, 395, 45.
- Rejkuba, M. 2004, *Å*, 413, 903.
- Rhee, M. and Chun, M. 1992, JKAS, 25, 11.
- Schiavon, R. P., Rose, J. A., Courteau, S., and MacArthur, L.A. 2005, ApJS, 160, 163.
- Schröder, L. L., Brodie, J. P., Kissler-Patig, M., Huchra, J. P., and Phillips, A. C. 2002, AJ, 123, 2473.
- Schlegel, D. J., Finkbeiner, D. P., and Davis, M. 1998, ApJ, 500, 525.
- Sharina, M. E., Afanasiev, V. L., and Puzia, T. H. 2006, MNRAS, 372, 1259.
- Sikkema, G., Peletier, R. F., Carter, D., Valentijn, E. A., and Balcells, M. 2006, *Å*, 458, 53.
- Strader, J., Brodie, J. P., and Forbes, D. A. 2004, AJ, 127, 295.
- Strader, J., Brodie, J. P., Forbes, D. A., Beasley, M. A., and Huchra, J. P. 2003, AJ, 125, 1291.
- Tonry J.L., Dressler A., Blakeslee J.P., Ajhar E. A., Fletcher A.B., Luppino G.A., Metzger M.R., and Moore C.B. 2001, ApJ, 546, 681.
- Trager, S. C., Worthey, G., Faber, S. M., Burstein, D., and Gonzalez, J. J. 1998, ApJS, 116, 1.
- Worthey, G., Faber, S. M., Gonzalez, J. J., and Burstein, D. 1994, ApJS, 95, 107.

- Xue, X.-X., Rix, H.-W., Zhao, G., Fiorentin, P. R., Naab, T., Steinmetz, M., van den Bosch, F. C., Beers, T. C., Lee, Y. S., Bell, E. F., Rockosi, C., Yanny, B., Newberg, H., Wilhelm, R., Kang, X., Smith, M. C., and Schneider, D. P. 2008, arXiv:0801.1232v4 [astro-ph]
- Zinn, R. 1985, ApJ, 283, 424.



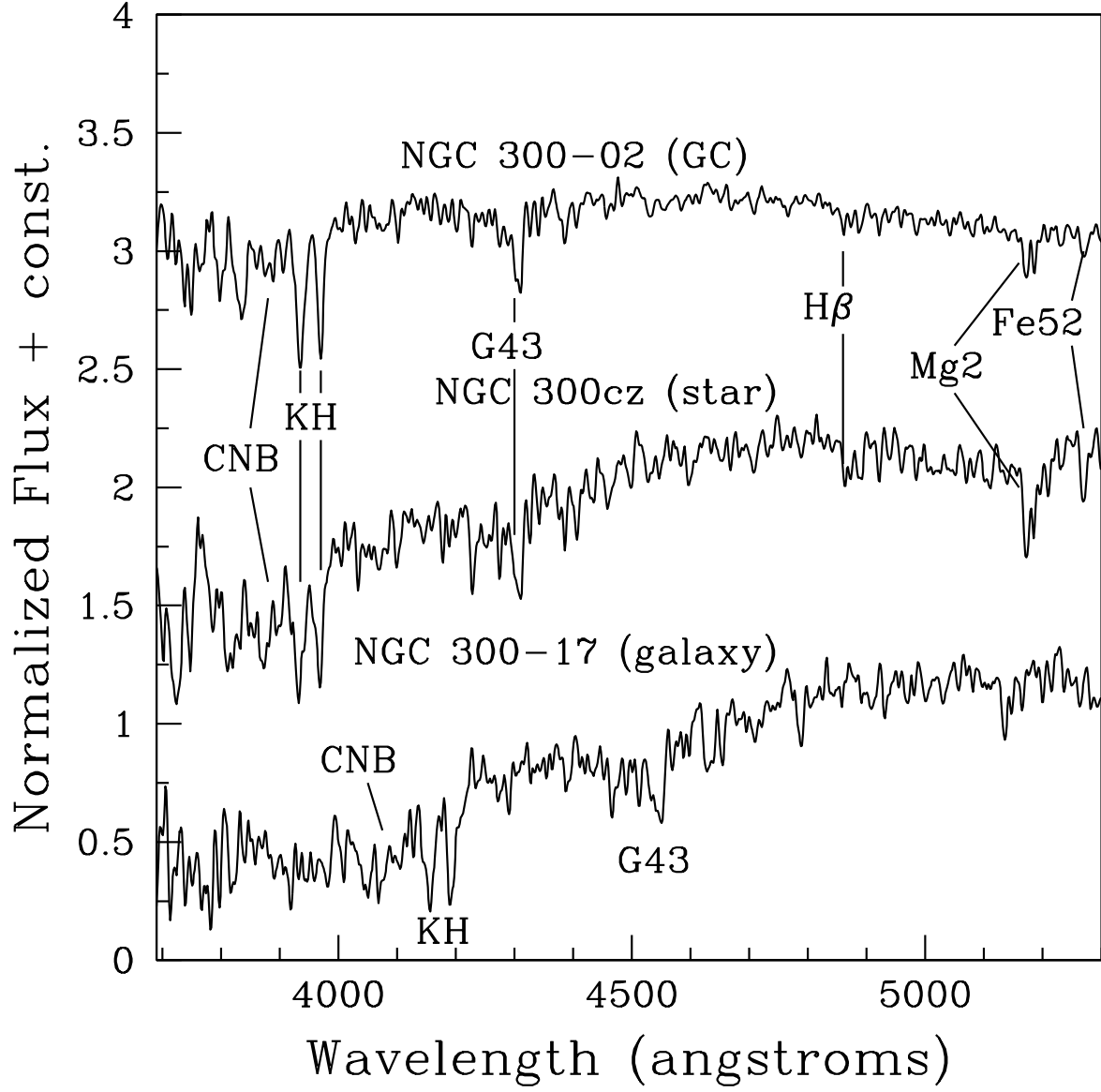


Fig. 2.— Sample spectrum of a globular cluster (top), a foreground star (middle), and a background galaxy (bottom), normalized and shown on the same scale.

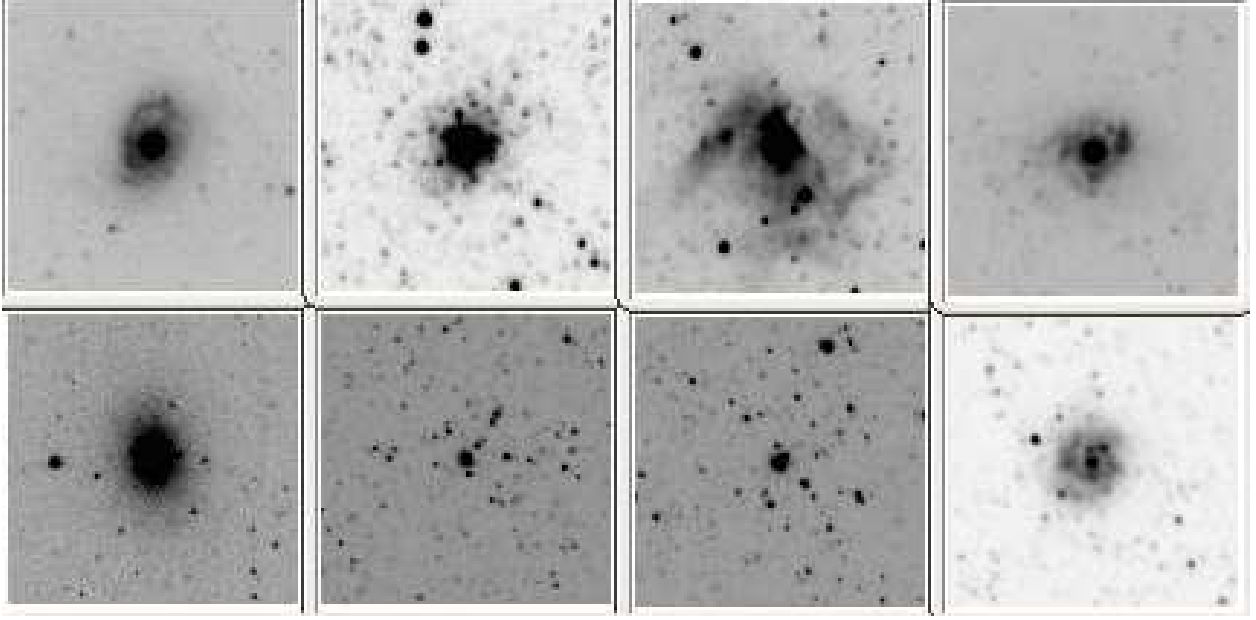


Fig. 3.— NGC 300 objects from the Kim et al. catalog found in the HST archives. On the top row, left to right, are Kim et al. Objects 1, 5, 6, and 7; on the bottom row, left to right, are Kim et al. objects 8, 9, 10, and 11.

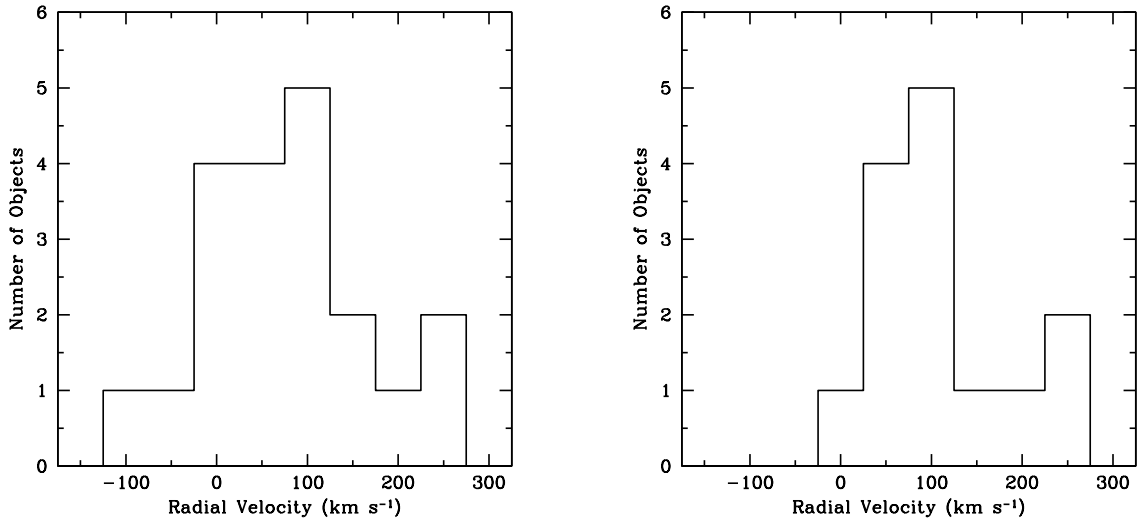


Fig. 4.— Velocity histogram of (a) all NGC 300 globular cluster candidates and (b) NGC 300 globular cluster candidates not labelled as “possible stars.”

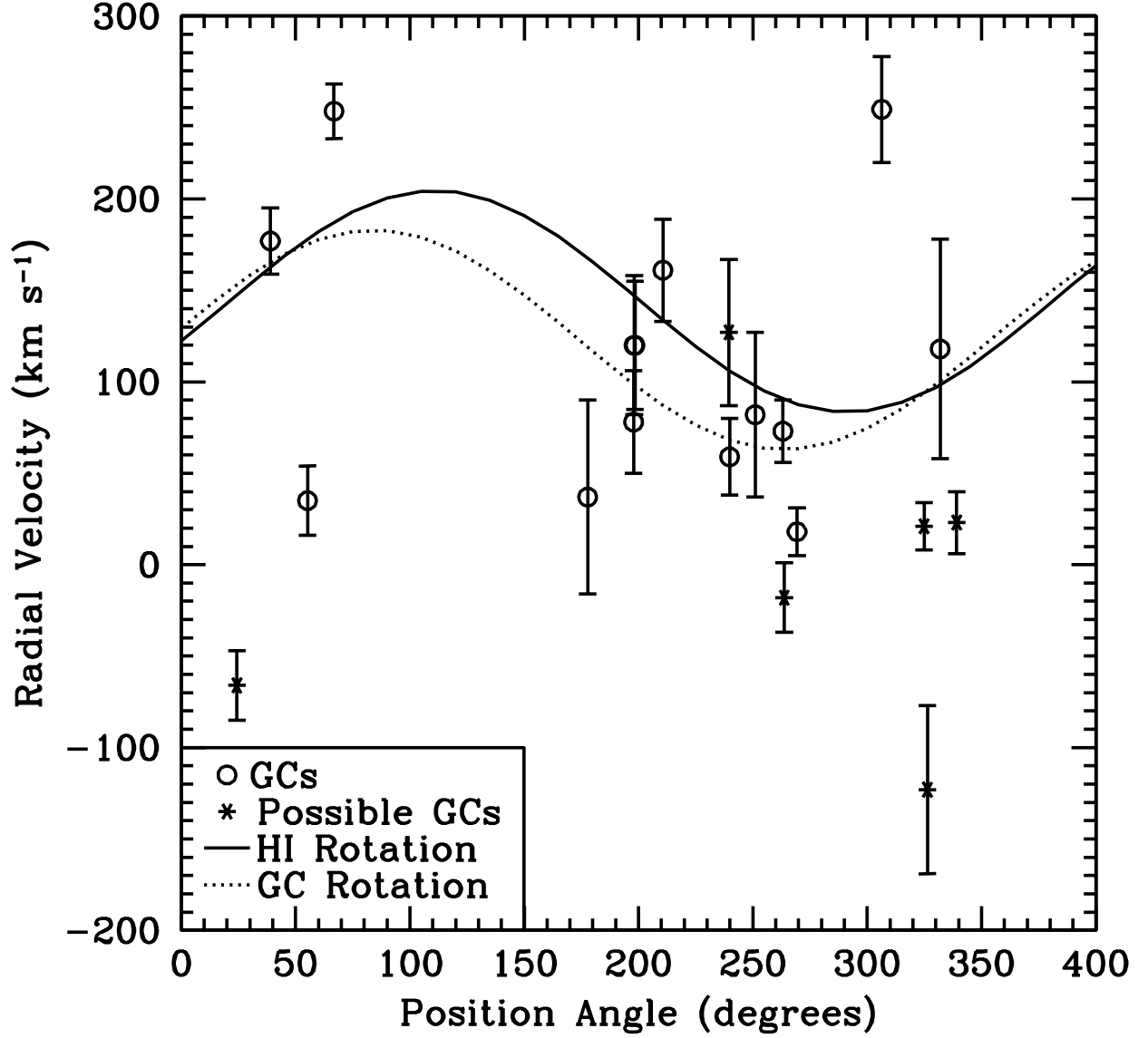


Fig. 5.— Velocity vs. position angle for the 14 highly probable GCs (open circles) and 6 possible GCs (stars), shown with a representation of the HI rotation curve (solid line) and a rotation curve calculated for the 14 highly probable GCs (dotted line).

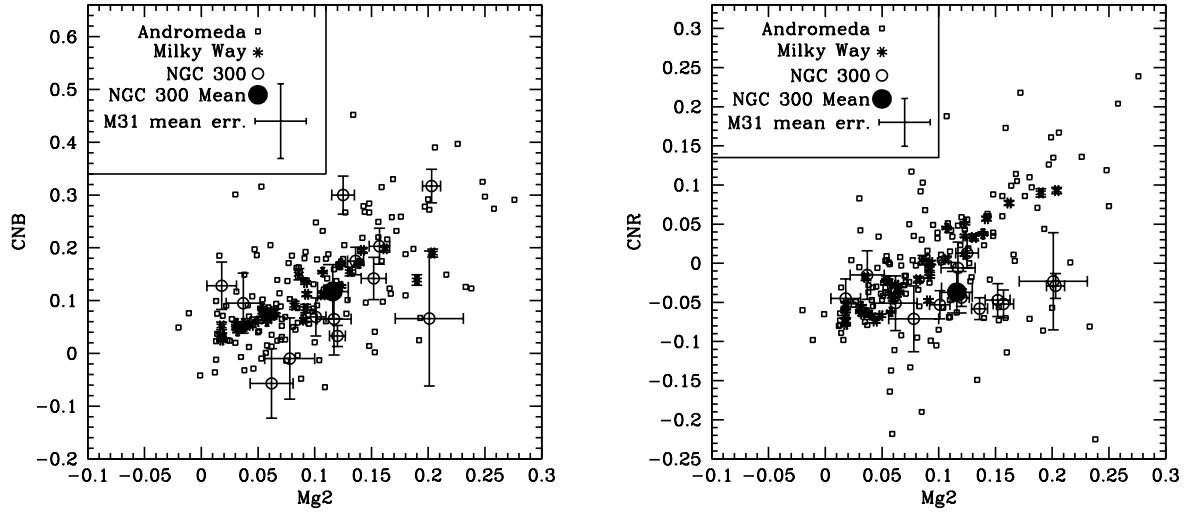


Fig. 6.— CN indices (blue on left, red on right) vs. Mg2 index. Open squares represent Andromeda clusters, asterisks represent Milky Way clusters, and open circles represent Sculptor Group clusters. A large filled circle marks the mean of NGC 300 clusters. The average error bar for M31 is shown in the legend. The average Milky Way uncertainty was smaller than the size of the symbols and therefore omitted.

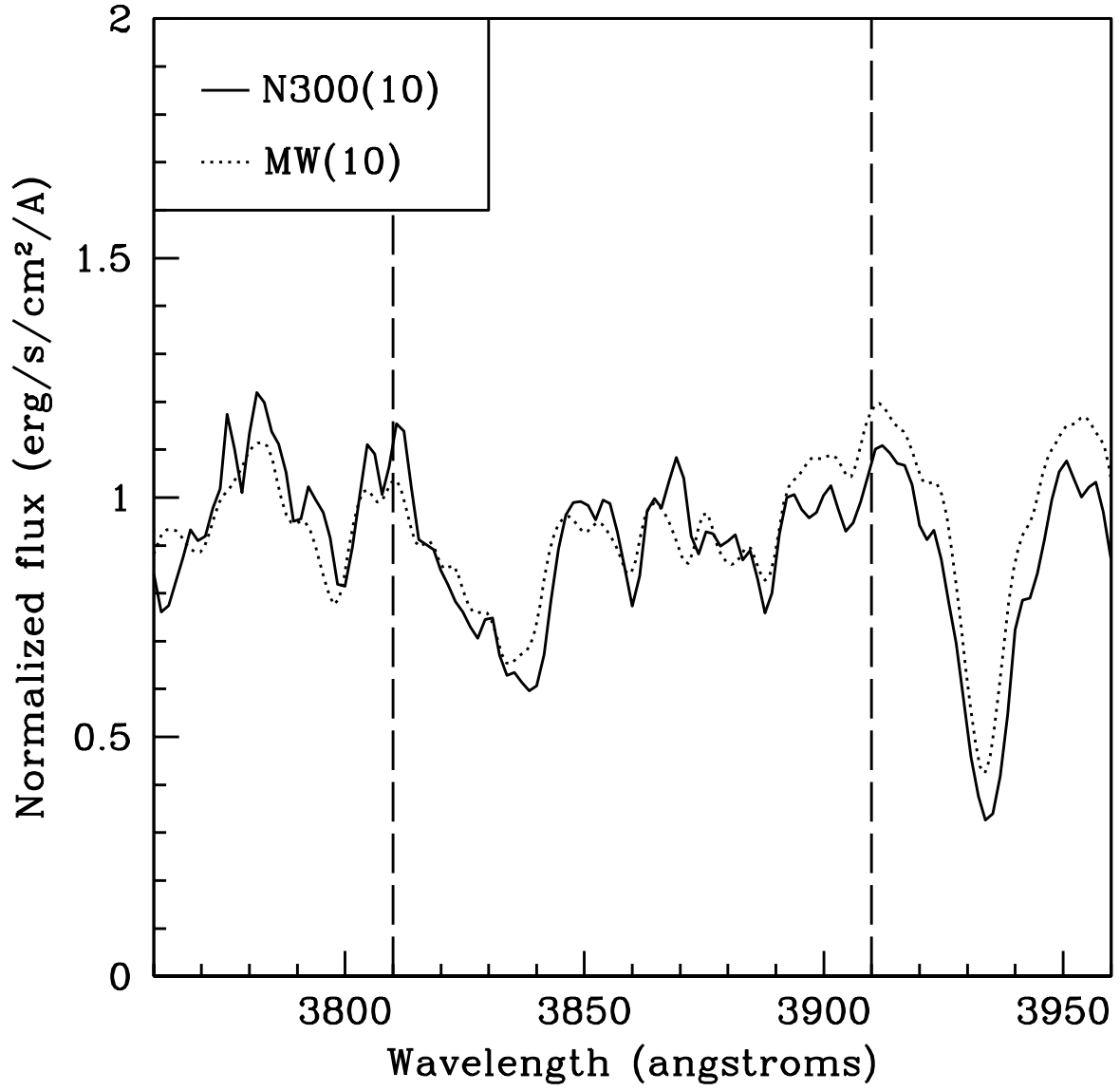


Fig. 7.— CNB feature for averages of 10 NGC 300 GCs and 10 MW GCs matched for Fe52 index strength.

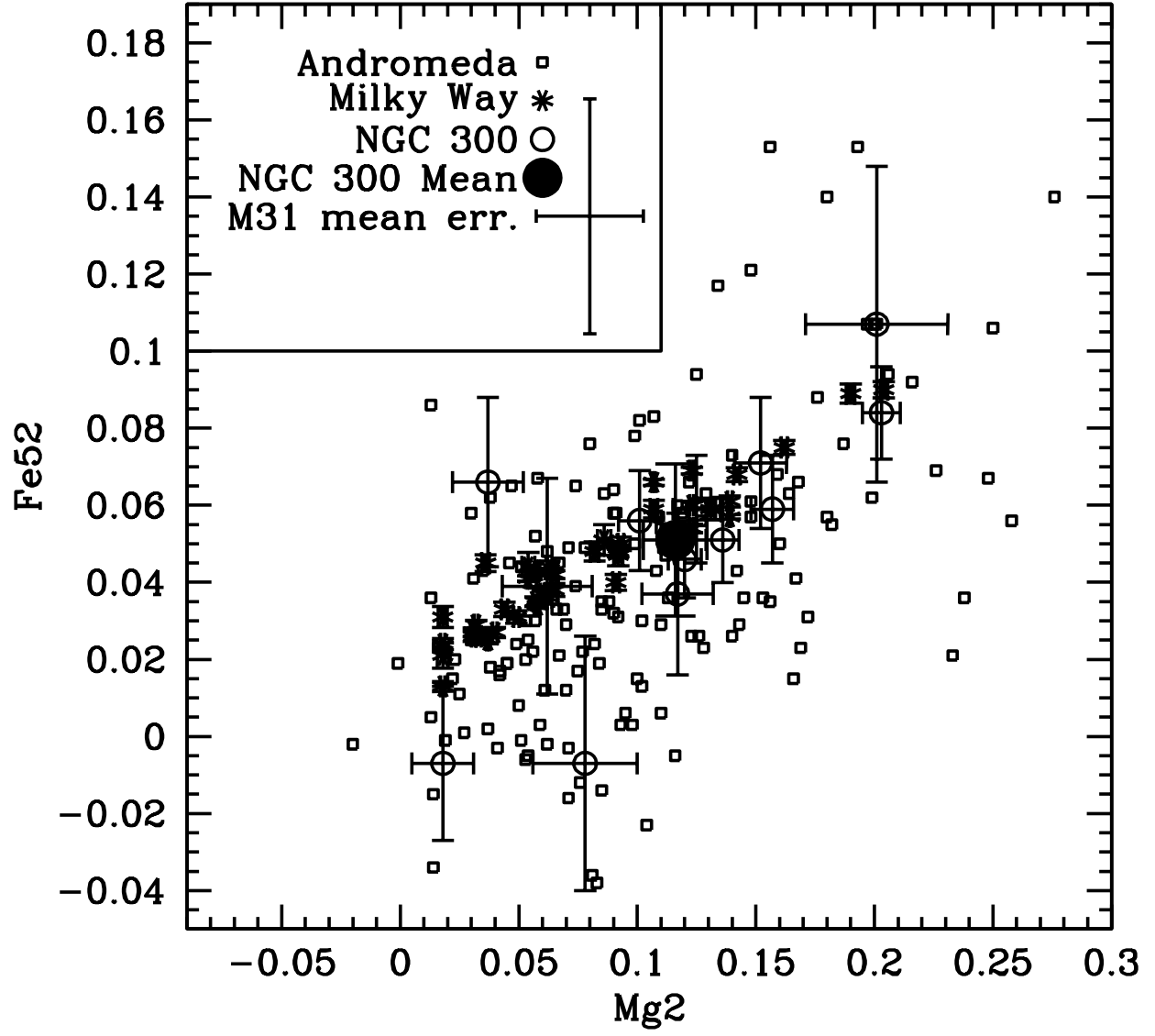


Fig. 8.— Fe-52 index vs. Mg2 index. Symbols are the same as in Figure 4.

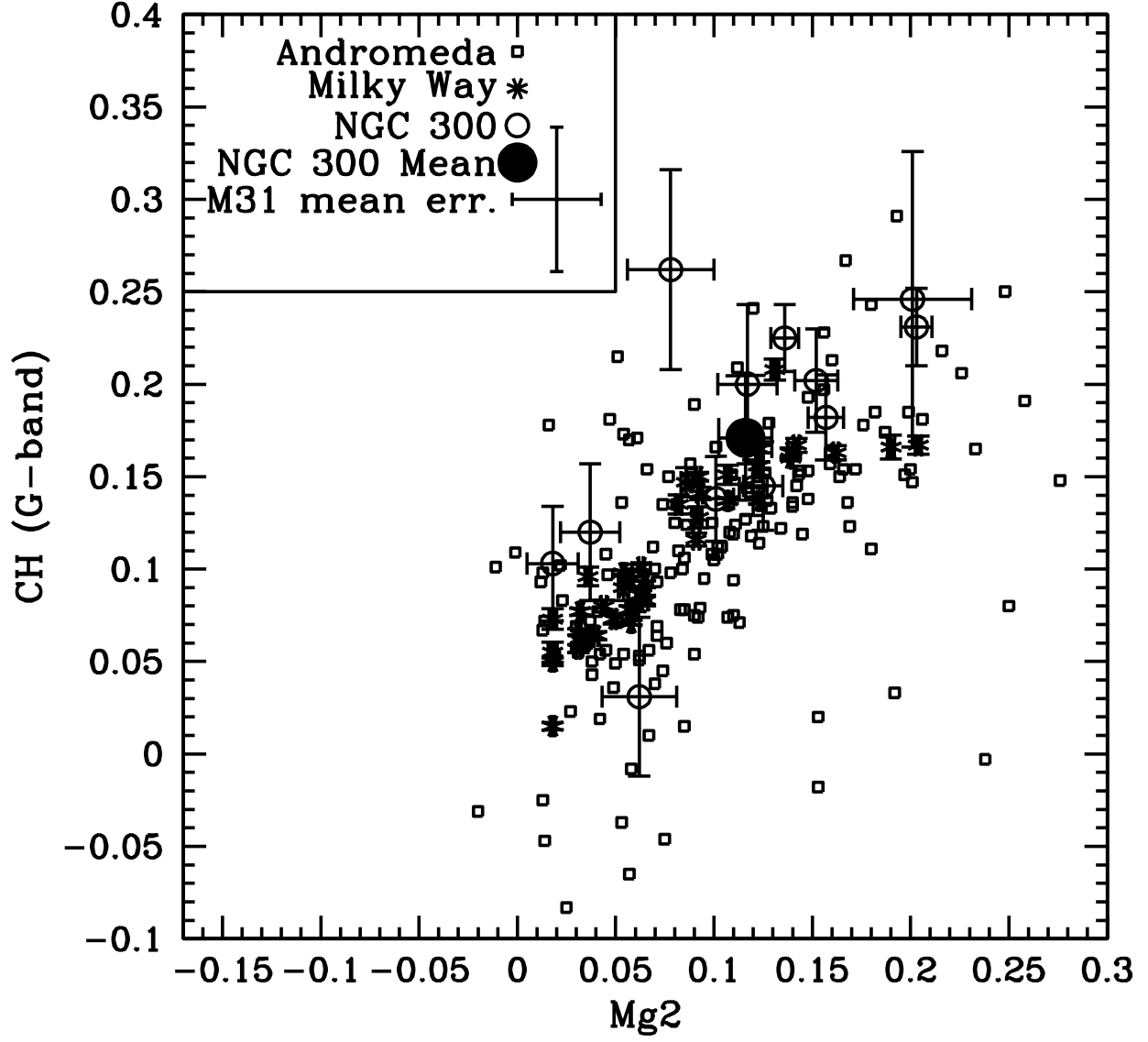


Fig. 9.— G-band (CH) index vs. Mg2 index. Symbols are the same as in Figure 4.

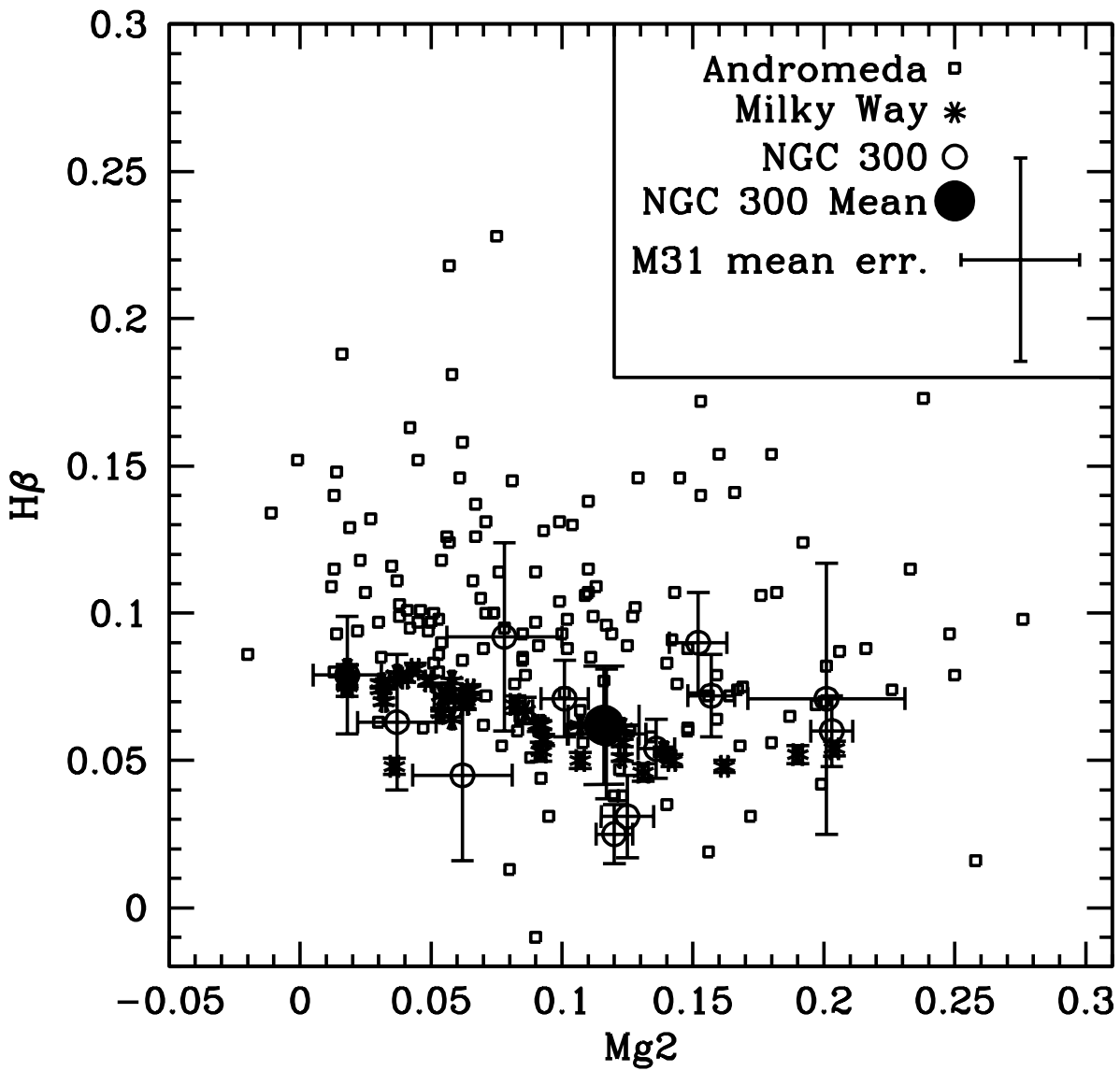


Fig. 10.— $H\beta$ index vs. Mg2 index. Symbols are the same as in Figure 4.

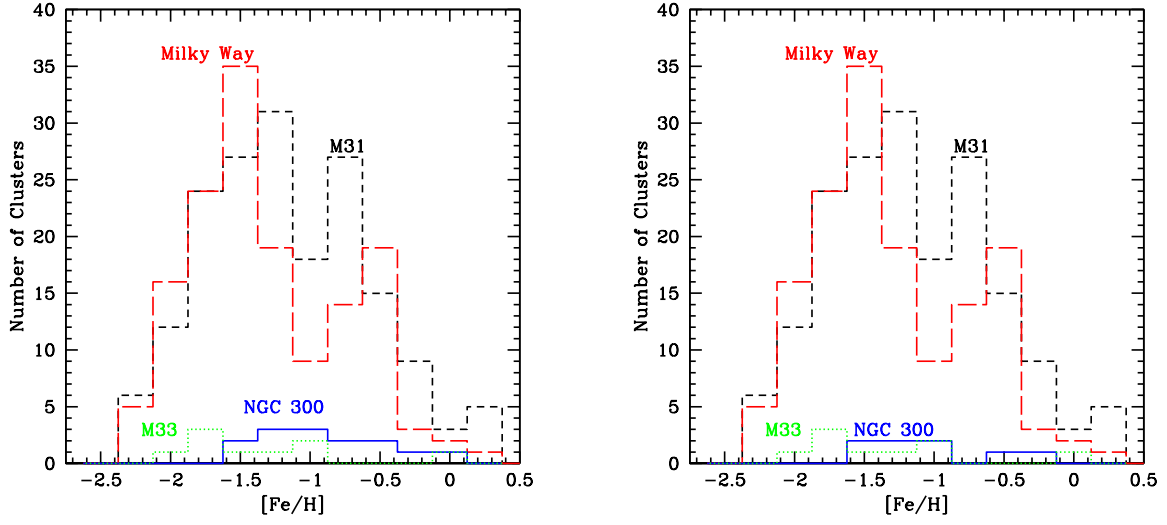


Fig. 11.— NGC 300 metallicity distributions, including (left) and not including (right) candidates flagged as possible stars. M31, M33, and Milky Way metallicity distributions are shown for comparison.

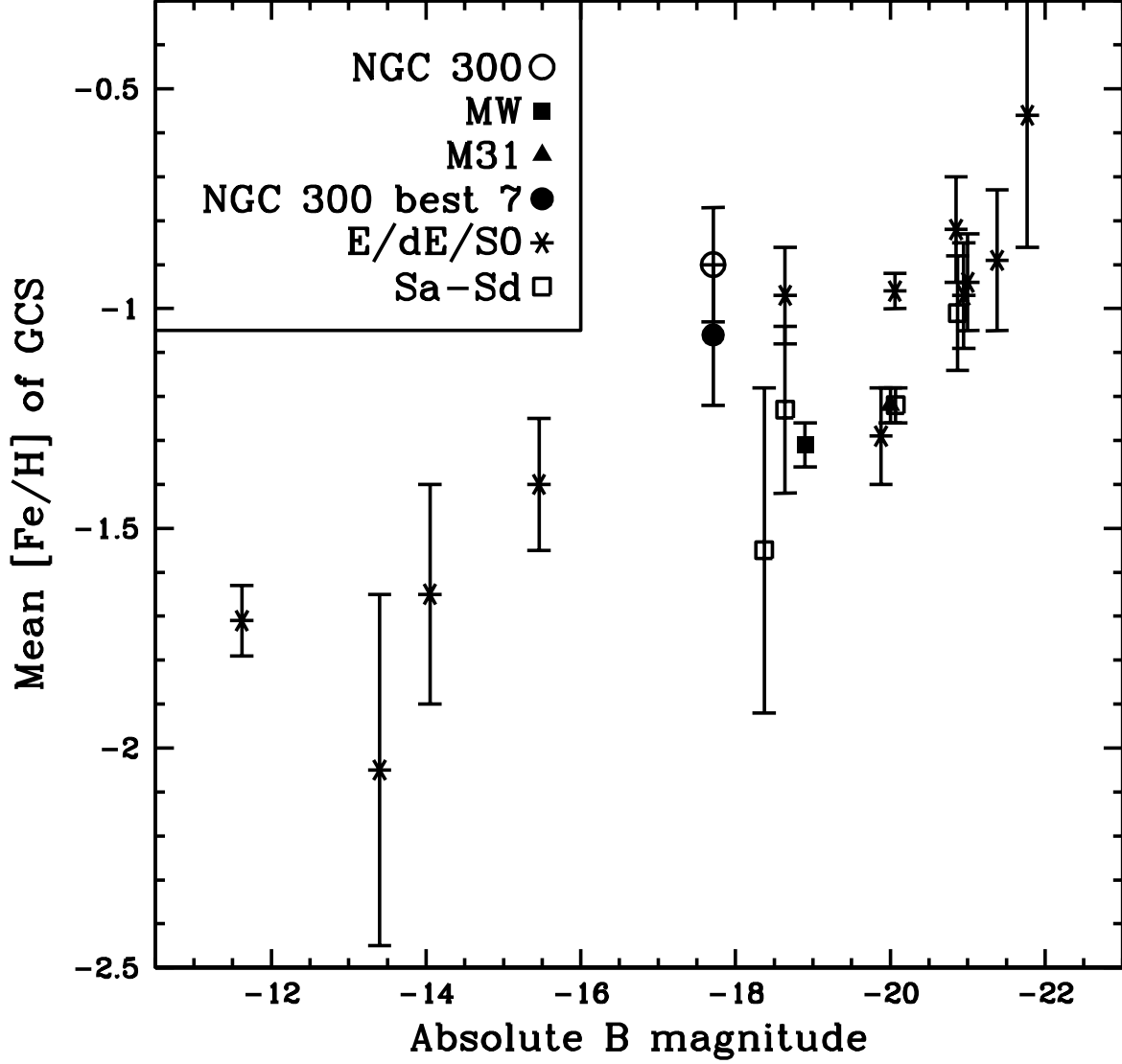


Fig. 12.— Average GCS metallicity vs. absolute B magnitude, showing NGC 300’s position including and excluding the “GC or star” objects and the possible young object. Color selection and small number statistics may make NGC 300’s globular cluster population appear disproportionately metal-rich compared to the Milky Way and Andromeda (the two points with the smallest error bars).

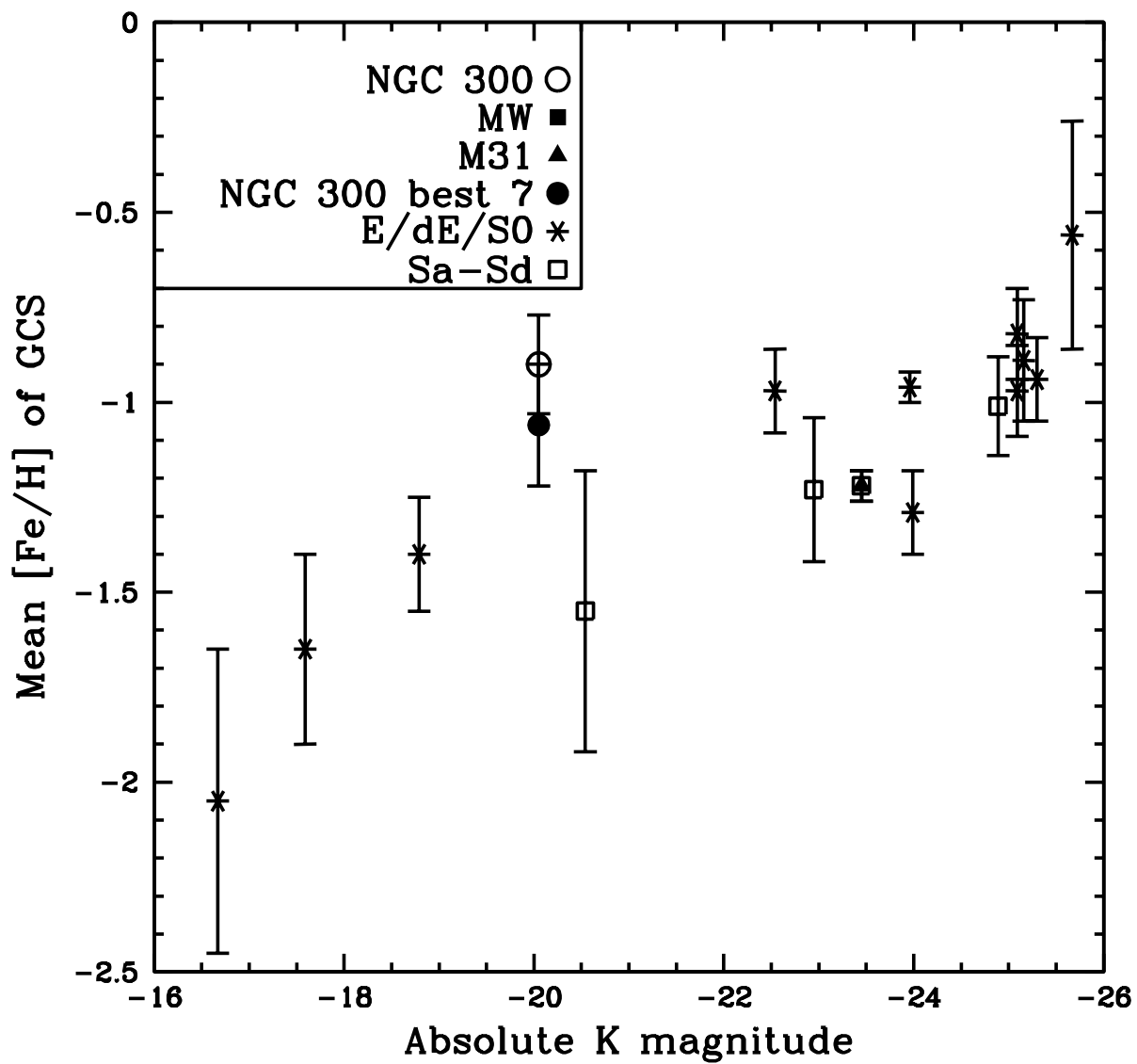


Fig. 13.— Average GCS metallicity vs. absolute K magnitude. Symbols are as in figure 8.

Table 1. Sculptor Velocities and Object Types from Spectra

Name	RA hh:mm:ss	DEC dd:mm:ss	K02 class	Velocity (km s ⁻¹)	Vel. err. (km s ⁻¹)	R-value	Template. ()	Object Type ()
NGC 253b	00:46:50.70	-25:26:38.90	–	209	43	7.87	m31_a_temp	gc
NGC 253ad	00:47:31.91	-25:26:42.53	–	65	40	7.42	fn4486btemp	gc
NGC 300cz	00:53:26.93	-37:41:55.54	–	81	19	16.6	fallstars	star
NGC 300cy	00:53:27.89	-37:55:21.48	–	85377	24	6.73	hemtemp0.0	(em.?)gal
NGC 300dt	00:53:40.30	-37:49:34.38	–	127	40	8.68	habtemp90	gc or star
NGC 300db	00:53:55.35	-37:23:42.98	–	-123	46	5.95	m31_f_temp	gc or star
NGC 300ds	00:53:56.12	-37:34:49.40	–	169	21	13.27	fabtemp97	star
NGC 300dd	00:53:56.47	-37:58:46.59	–	11483	29	4.26	hemtemp0.0	gal?
NGC 300cm	00:54:05.51	-37:42:06.11	–	-18	19	14.24	m31_k_temp	gc or star
NGC 300-01	00:54:22.07	-37:43:22.1	1	49374	34	8.78	habtemp90	gal*
NGC 300ck	00:54:21.84	-37:32:07.82	–	21	13	19.27	fallstars	gc or star
NGC 300cj	00:54:24.13	-37:25:46.17	–	23	17	15.63	m31_k_temp	gc or star
NGC 300-08	00:54:57.41	-37:33:55.30	2	16797	22	14.43	habtemp90	gal*
NGC 300-02	00:54:35.80	-37:43:05.60	2	59	21	15.11	habtemp90	gc
NGC 300-15	00:55:21.81	-37:45:40.10	2	106	22	20.12	m31_a_temp	star
NGC 300-03	00:54:40.02	-37:49:18.71	3	78	28	10.04	m31_f_temp	gc
NGC 300-04	00:54:45.62	-37:43:41.00	2	161	28	9.14	m31_f_temp	gc
NGC 300-14	00:55:17.67	-37:36:57.90	2	16995	36	8.68	fallstars	gal
NGC 300-05	00:54:49.35	-37:43:30.50	2	120	35	8.08	m31_f_temp	gc*
NGC 300-09	00:54:57.57	-37:36:37.90	2	214	14	18.08	fglotemp	star*
NGC 300-11	00:55:01.44	-37:37:21.80	1	38350	17	8.83	hemtemp0.0	em.gal*
NGC 300cl	00:54:53.85	-37:23:57.44	–	21	16	17.4	fabtemp97	star
NGC 300dc	00:54:54.66	-37:58:34.98	–	68066	25	5.13	hemtemp0.0	em.gal
NGC 300df	00:54:57.02	-37:58:52.21	–	37	53	5.76	m31_k_temp	gc
NGC 300-10	00:54:59.03	-37:36:24.40	3	173	23	12.59	m31_f_temp	star*
NGC 300ax	00:55:01.49	-37:47:36.40	–	-27	32	8.43	m31_k_temp	star
NGC 300-07	00:54:53.22	-37:43:11.1	1	43722	27	6.41	hemtemp0.0	em.gal*
NGC 300-12	00:55:11.03	-37:36:46.10	1	177	18	15.19	m31_f_temp	gc
NGC 300co	00:55:19.49	-37:29:38.73	–	-66	19	14.57	m31_k_temp	gc or star
NGC 300-06	00:54:51.67	-37:39:38.00	3	156	14	8.97	hemtemp0.0	HII*
NGC 300-17	00:55:38.79	-37:46:30.70	3	16868	21	13.02	fallstars	gal
NGC 300-16	00:55:27.56	-37:46:09.40	3	16798	29	8.03	m31_k_temp	gal
NGC 300-13	00:55:11.17	-37:33:13.90	3	38182	20	6.19	hemtemp0.0	em.gal
NGC 300cr	00:55:52.72	-37:59:04.14	–	-23	15	17.05	fallstars	star
NGC 300bd	00:55:56.79	-37:52:07.28	–	68818	20	6.69	hemtemp0.0	gal
NGC 300cq	00:56:07.09	-37:57:02.64	–	-79	14	17.25	fallstars	star
NGC 300cs	00:56:07.62	-37:57:23.07	–	31	16	15.85	fallstars	star
NGC 300da	00:56:09.49	-37:31:21.25	–	49619	21	7.51	hemtemp0.0	em.gal
NGC 300cv	00:56:13.97	-37:34:16.27	–	97	17	12.33	fabtemp97	star
NGC 300ct	00:56:18.24	-37:28:48.08	–	4	15	17.59	fabtemp97	star
NGC 300cp	00:56:19.03	-37:29:17.23	–	35	19	13.88	m31_k_temp	gc
NGC 300cx	00:56:20.30	-37:59:11.68	–	68618	53	5.97	m31_f_temp	gal
NGC 300cn	00:56:23.52	-37:27:37.57	–	49828	17	8.89	hemtemp0.0	em.gal
NGC 300cu	00:56:24.62	-37:52:56.29	–	18	20	12.33	fallstars	star

Note. — Objects with letter designations (e.g. NGC 300cx) are from Olsen et al. (2004). Objects with number designations (e.g. NGC 300-05) are from Kim et al. (2002). Objects with asterisks next to the object type have been visually inspected in archival HST images.

Table 2. Velocities of Globular Cluster Candidates

ID	RA (J2000) (hours)	Dec (J2000) (minutes)	RV (km s ⁻¹)	σ_{RV} (km s ⁻¹)	Object type	Vel. source
NGC 300ac	00:54:02.48	-37:44:31.64	82	45	gc	Olsen et al. 2004
NGC 300ag	00:54:23.22	-37:59:17.67	120	38	gc	Olsen et al. 2004
NGC 300am	00:54:07.54	-37:42:09.23	73	17	gc	Olsen (unpublished)
NGC 300ba	00:54:05.49	-37:23:11.24	118	60	gc	Olsen et al. 2004
NGC 300m	00:54:07.04	-37:41:10.35	18	13	gc	Olsen (unpublished)
NGC 300r	00:56:23.13	-37:33:26.98	248	15	gc	Olsen et al. 2004
NGC 300s	00:53:55.66	-37:32:37.38	249	29	gc	Olsen et al. 2004
NGC 300-03	00:54:40.02	-37:49:18.71	78	28	gc	this paper
NGC 300-04	00:54:45.62	-37:43:41.00	161	28	gc	this paper
NGC 300-02	00:54:35.80	-37:43:05.60	59	21	gc	this paper
NGC 300cp	00:56:19.03	-37:29:17.23	35	19	gc	this paper
NGC 300-12	00:55:11.03	-37:36:46.10	177	18	gc	this paper
NGC 300-05	00:54:49.35	-37:43:30.50	120	35	gc	this paper
NGC 300df	00:54:57.02	-37:58:52.21	37	53	gc	this paper
NGC 300co	00:55:19.49	-37:29:38.73	-66	19	gc or star	this paper
NGC 300cm	00:54:05.51	-37:42:06.11	-18	19	gc or star	this paper
NGC 300db	00:53:55.35	-37:23:42.98	-123	46	gc or star	this paper
NGC 300dt	00:53:40.30	-37:49:34.38	127	40	gc or star	this paper
NGC 300cj	00:54:24.13	-37:25:46.17	23	17	gc or star	this paper
NGC 300ck	00:54:21.84	-37:32:07.82	21	13	gc or star	this paper

Table 3. Brodie & Huchra Calibrated Spectral Indices

Name	CNR mag	CH/G mag	H β mag	MgH mag	Mg2 mag	Mgb mag	Fe52 mag	NaI mag	CNB mag	H&K mag	MgG mag	δ mag
NGC 253ad	0.017	0.262	0.039	0.048	0.177	0.152	0.027	0.046	0.294	0.312	-0.086	0.477
σ	0.058	0.069	0.036	0.022	0.025	0.042	0.034	0.040	0.116	0.117	0.067	0.030
NGC 253b	-0.132	0.037	0.058	0.009	0.017	0.005	-0.005	0.049	0.216	0.234	-0.088	0.252
σ	0.041	0.051	0.032	0.019	0.021	0.035	0.031	0.040	0.068	0.065	0.048	0.018
NGC 300-02	-0.044	0.144	0.025	0.001	0.120	0.110	0.046	0.039	0.033	0.216	0.001	0.244
σ	0.011	0.015	0.010	0.006	0.007	0.012	0.010	0.013	0.020	0.019	0.015	0.005
NGC 300-03	-0.045	0.103	0.079	-0.008	0.018	0.045	-0.007	0.035	0.128	0.312	-0.188	0.298
σ	0.025	0.031	0.020	0.012	0.013	0.023	0.020	0.028	0.045	0.042	0.034	0.012
NGC 300-04	-0.015	0.120	0.063	0.010	0.037	0.064	0.066	0.008	0.095	0.328	-0.165	0.354
σ	0.031	0.037	0.023	0.014	0.015	0.025	0.022	0.029	0.057	0.056	0.039	0.014
NGC 300-05	-0.051	0.031	0.045	0.007	0.062	0.086	0.039	-0.047	-0.057	0.184	-0.134	0.243
σ	0.035	0.043	0.029	0.017	0.019	0.032	0.028	0.042	0.066	0.061	0.050	0.015
NGC 300-12	-0.053	0.138	0.071	0.030	0.101	0.088	0.056	0.026	0.069	0.362	-0.245	0.446
σ	0.018	0.023	0.013	0.008	0.009	0.015	0.013	0.016	0.036	0.033	0.025	0.009
NGC 300cj	-0.058	0.225	0.054	0.012	0.136	0.136	0.051	0.049	0.175	0.399	-0.187	0.536
σ	0.014	0.018	0.010	0.006	0.007	0.012	0.011	0.012	0.026	0.025	0.018	0.007
NGC 300ck	-0.029	0.231	0.060	0.030	0.203	0.180	0.084	0.070	0.317	0.378	-0.200	0.664
σ	0.016	0.021	0.012	0.007	0.008	0.014	0.012	0.013	0.032	0.029	0.023	0.008
NGC 300cm	-0.052	0.182	0.072	0.022	0.157	0.160	0.059	0.036	0.203	0.350	-0.108	0.483
σ	0.018	0.023	0.014	0.008	0.009	0.016	0.014	0.016	0.034	0.033	0.023	0.009
NGC 300co	0.013	0.145	0.031	0.013	0.125	0.121	0.059	0.060	0.300	0.434	-0.181	0.561
σ	0.019	0.024	0.014	0.009	0.010	0.017	0.014	0.016	0.036	0.035	0.025	0.009
NGC 300cp	-0.047	0.202	0.090	-0.001	0.152	0.166	0.071	0.027	0.142	0.375	-0.082	0.460
σ	0.021	0.028	0.017	0.010	0.011	0.019	0.017	0.020	0.040	0.039	0.028	0.010
NGC 300db	-0.071	0.262	0.092	0.002	0.078	0.114	-0.007	-0.026	-0.010	0.268	-0.022	0.226
σ	0.042	0.054	0.032	0.020	0.022	0.037	0.033	0.041	0.077	0.074	0.055	0.019
NGC 300df	-0.023	0.246	0.071	0.009	0.201	0.152	0.107	0.141	0.066	0.257	-0.025	0.261
σ	0.062	0.080	0.046	0.026	0.030	0.053	0.041	0.054	0.128	0.118	0.090	0.032
NGC 300dt	-0.006	0.200	0.059	0.008	0.117	0.177	0.037	0.087	0.065	0.268	-0.024	0.269
σ	0.033	0.043	0.022	0.013	0.015	0.025	0.021	0.028	0.068	0.063	0.045	0.016
<NGC 300>	-0.037	0.171	0.062	0.010	0.116	0.123	0.051	0.039	0.117	0.318	-0.120	0.388
σ	0.007	0.009	0.006	0.003	0.004	0.006	0.005	0.007	0.014	0.013	0.010	0.003

Note. — CNR \sim Lick/IDS CN1; MgH \sim Lick/IDS Index Mg1; NaI \sim Lick/IDS index NaD. All other indices correspond to the Lick/IDS indices of the same name. CNB, H&K, MgG, and δ have no Lick/IDS equivalents..

Table 4. Other Spectral Indices

Name	CN2 mag	Ca42 mag	Fe43 mag	Ca44 mag	Fe45 mag	C2 mag	Fe50 mag	Fe53 mag	Fe54 mag	Fe5709 mag	Fe5782 mag	TiO1 mag	TiO2 mag
NGC 253ad	0.041	0.102	0.088	0.048	0.056	0.060	0.052	0.036	0.036	0.058	-0.014	0.008	0.028
σ	0.074	0.102	0.064	0.065	0.054	0.041	0.036	0.043	0.043	0.037	0.044	0.024	0.022
NGC 253b	-0.104	-0.048	0.001	0.049	0.075	0.067	0.001	-0.029	-0.029	0.001	-0.021	-0.010	0.008
σ	0.053	0.073	0.051	0.051	0.044	0.035	0.032	0.040	0.040	0.036	0.042	0.023	0.022
NGC 300-02	-0.030	0.066	0.067	0.032	0.046	0.013	0.032	0.047	0.047	0.018	0.022	0.009	0.012
σ	0.015	0.020	0.014	0.015	0.013	0.011	0.010	0.013	0.013	0.012	0.015	0.008	0.008
NGC 300-03	-0.021	0.072	-0.020	0.023	0.081	0.024	0.046	-0.008	-0.008	0.019	-0.019	-0.032	0.007
σ	0.033	0.044	0.032	0.031	0.027	0.022	0.020	0.026	0.026	0.024	0.028	0.015	0.015
NGC 300-04	-0.026	0.072	0.060	0.028	0.069	0.044	0.065	0.052	0.052	0.038	0.024	0.007	0.011
σ	0.041	0.055	0.037	0.038	0.032	0.025	0.023	0.028	0.028	0.026	0.032	0.017	0.016
NGC 300-05	-0.052	0.081	-0.004	-0.045	0.003	0.012	-0.017	0.031	0.031	-0.025	-0.047	0.005	0.016
σ	0.047	0.060	0.044	0.046	0.039	0.030	0.029	0.036	0.036	0.035	0.042	0.023	0.022
NGC 300-12	-0.023	0.102	0.064	0.030	0.069	0.027	0.036	0.040	0.040	0.023	0.022	0.042	0.064
σ	0.024	0.032	0.021	0.022	0.018	0.015	0.014	0.017	0.017	0.015	0.018	0.010	0.010
NGC 300cj	-0.036	0.069	0.096	0.050	0.067	0.039	0.050	0.041	0.041	0.027	0.013	-0.009	0.009
σ	0.018	0.024	0.017	0.017	0.014	0.012	0.011	0.013	0.013	0.012	0.014	0.008	0.008
NGC 300ck	0.011	0.147	0.120	0.069	0.072	0.050	0.068	0.077	0.077	0.016	0.030	0.001	0.017
σ	0.020	0.028	0.018	0.019	0.016	0.013	0.012	0.015	0.015	0.013	0.016	0.009	0.009
NGC 300cm	-0.026	0.144	0.083	0.071	0.053	0.004	0.026	0.052	0.052	0.001	0.030	0.020	0.005
σ	0.023	0.032	0.021	0.022	0.019	0.015	0.014	0.017	0.017	0.016	0.019	0.010	0.010
NGC 300co	0.039	0.124	0.039	0.041	0.049	0.012	0.044	0.039	0.039	0.023	0.019	-0.001	0.008
σ	0.024	0.034	0.022	0.024	0.020	0.016	0.015	0.018	0.018	0.016	0.019	0.010	0.010
NGC 300cp	-0.009	0.110	0.039	0.045	0.055	0.038	0.037	0.044	0.044	0.001	0.023	-0.008	0.015
σ	0.027	0.038	0.026	0.027	0.022	0.018	0.017	0.021	0.021	0.019	0.023	0.012	0.012
NGC 300db	-0.043	0.091	-0.023	-0.004	-0.061	0.016	0.022	0.043	0.043	-0.025	-0.080	-0.058	-0.021
σ	0.055	0.072	0.054	0.055	0.046	0.037	0.034	0.040	0.040	0.037	0.045	0.024	0.024
NGC 300df	0.016	0.294	0.071	0.020	0.047	-0.023	0.087	0.059	0.059	0.068	-0.088	-0.016	-0.054
σ	0.081	0.110	0.072	0.072	0.061	0.049	0.042	0.050	0.050	0.045	0.058	0.030	0.030
NGC 300dt	0.000	0.131	0.134	0.088	0.063	-0.006	0.037	0.009	0.009	0.025	-0.048	-0.021	0.002
σ	0.043	0.055	0.036	0.036	0.031	0.025	0.022	0.027	0.027	0.024	0.029	0.016	0.015
<NGC 300>	-0.015	0.116	0.056	0.034	0.047	0.019	0.041	0.041	0.038	0.016	-0.008	-0.005	0.007
σ	0.010	0.013	0.009	0.009	0.008	0.006	0.006	0.007	0.007	0.006	0.008	0.004	0.004

Table 5. Linear Fits to $[Fe/H] = a(index) + b$

Index ID	a (dex/mag)	b (dex)	R^2	R_I	σ_m	σ_s
Ca4455	25.85	-2.00	0.899	0.0387	0.006	0.003
Fe5270	26.50	-2.31	0.888	0.0377	0.006	0.001
Mg2	9.83	-1.89	0.886	0.1017	0.017	0.006
δ	4.12	-2.68	0.884	0.2428	0.041	0.095
Fe5335	30.36	-2.22	0.879	0.0329	0.006	0.005
Ca4227	18.65	-2.09	0.878	0.0536	0.010	0.014
CN2	9.45	-1.27	0.852	0.1058	0.020	0.021
G4300	10.37	-2.24	0.844	0.0964	0.019	0.008

Table 6. Sculptor Globular Cluster Metallicities

Name	[Fe/H] dex	$\sigma_{[Fe/H]}$ dex	[Fe/H] Src.	Ols. No.
NGC 55az	-1.76	0.43	Ols	27
NGC 253q	-1.07	0.30	Ols	5
NGC 253b	-1.96	0.54	new	26
NGC 247a	-1.04	0.29	Ols	64
NGC 253a	-0.88	0.25	Ols	46
NGC 253ad	-0.52	0.56	new	57
NGC 300dt	-0.89	0.66	new	13
NGC 300db	-1.23	0.82	new	22
NGC 300cm	-0.54	0.36	new	33
NGC 300ck	-0.07	0.25	new	42
NGC 300cj	-0.71	0.35	new	45
NGC 300-02	-1.03	0.29	new	n/a
NGC 300-03	-1.61	0.47	new	48
NGC 300-04	-1.17	0.33	new	n/a
NGC 300-05	-1.57	0.53	new	n/a
NGC 300df	-0.33	1.12	new	61
NGC 300-12	-0.93	0.23	new	n/a
NGC 300co	-0.67	0.29	new	69
NGC 300cp	-0.59	0.29	new	116
NGC 300r	-1.25	0.35	Ols	121

Note. — Ols.No. is the object number in Olsen et al. (2004) Table 4. Src. designates the source of the metallicity value: "Ols" for Olsen et al. (2004) or "new" for the newly reduced spectra. Be careful using the "metallicity" for NGC 300-10, as it is likely young.

Table 7. Mean Galaxy GCS Metallicities and Luminosities

ID	$\langle [m/H] \rangle$ (dex)	$\sigma_{\langle [m/H] \rangle}$ (dex)	B_t (mag)	Distance (Mpc)	M_{Bt} (mag)	K (mag)	M_K (mag)	Ref-Metal	Ref-Dist.	Ref-K
Fornax	-1.71	0.08	9.28	0.136	-11.38	–	–	32	5	–
M87	-0.89	0.16	9.56	15.631	-21.38	5.81	-25.16	6	11	17
M31	-1.22	0.04	4.36	0.77	-20.07	0.98	-23.45	2	12	17
MW	-1.31	0.05	5.52	0.76	-18.9	–	–	16	–	–
M81	-1.19	0.14	7.89	3.6	-19.89	3.83	-23.95	29, 26	13	17
M33	-1.55	0.37	6.27	0.847	-18.37	4.1	-20.54	6	14	17
M49	-0.56	0.3	9.37	16.368	-21.7	5.4	-25.67	9	11	17
N 147	-2.05	0.4	10.47	0.594	-13.4	7.2	-16.67	6	19	17
N 205	-1.40	0.15	8.92	0.752	-15.46	5.59	-18.79	6	30	17
N 185	-1.65	0.25	10.1	0.676	-14.05	6.56	-17.59	6	23	17
M104	-1.01	0.13	8.98	9.333	-20.87	4.96	-24.89	22	11	17
N 5128	-0.96	0.04	7.84	3.8	-20.06	3.94	-23.96	3	28	17
N 2683	-1.23	0.19	10.64	7.178	-18.64	6.33	-22.95	27	33, 18	17
N 7457	-0.97	0.11	12.09	13.996	-18.64	8.19	-22.54	8	11, 7	1
N 1023	-1.29	0.11	10.35	11.117	-19.88	6.24	-23.99	21	11	17
N 1399	-0.82	0.12	10	19.055	-21.4	6.31	-25.09	20	11	17
N 3923	-0.94	0.11	10.8	22.909	-21.0	6.5	-25.3	24	31	17
N 524	-0.97	0.12	11.3	28.2	-20.95	7.16	-25.09	4	10	1
N 300	-0.90	0.13	8.95	1.93	-17.48	6.38	-20.05	25, this paper	15	17

References. — (1) 2MASS Extended Source Catalog; (2) Barmby et al. 2000; (3) Beasley et al. 2008; (4) Beasley et al. 2004; (5) Bersier 2000; (6) Brodie and Huchra 1991; (7) Cappellari et al. 2006; (8) Chomiuk, Strader, and Brodie 2008; (9) Cohen, Blakeslee, and Coté 2003; (10) de Vaucouleurs et al. 1991; (11) Ferrarese et al. 2000; (12) Freedman 1990; (13) Freedman et al. 1994; (14) Galleti, Bellazzini, and Ferraro 2004; (15) Gieren et al. 2004; (16) Harris et al. 1996; (17) Jarrett et al. 2003; (18) Jensen et al. 2003; (19) Kang et al. 2007; (20) Kissler-Patig et al. 1998; (21) Larsen and Brodie 2002; (22) Larsen et al. 2002; (23) McConnachie et al. 2004; (24) Norris et al. 2008; (25) Olsen et al. 2004; (26) Perelmuter, Brodie, and Huchra 1995; (27) Proctor et al. 2008; (28) Rejkuba 2004; (29) Schröder et al. 2002; (30) Sharina, Afanasiev, and Puzia 2006; (31) Sikkema et al. 2006; (32) Strader et al. 2003; (33) Tonry et al. 2001.